COMPUTATIONAL BIOLOGY

Multiplexed gene control reveals rapid mRNA turnover

Antoine Baudrimont,* Sylvia Voegeli,* Eduardo Calero Viloria,* Fabian Stritt, Marine Lenon, Takeo Wada, Vincent Jaquet, Attila Becskei†

The rates of mRNA synthesis and decay determine the mRNA expression level. The two processes are under coordinated control, which makes the measurements of these rates challenging, as evidenced by the low correlation among the methods of measurement of RNA half-lives. We developed a minimally invasive method, multiplexed gene control, to shut off expression of genes with controllable synthetic promoters. The method was validated by measuring the ratios of the nascent to mature mRNA molecules and by measuring the half-life with endogenous promoters that can be controlled naturally or through inserting short sequences that impart repressibility. The measured mRNA half-lives correlated highly with those obtained with the metabolic pulse-labeling method in yeast. However, mRNA degradation was considerably faster in comparison to previous estimates, with a median half-life of around 2 min. The half-life permits the estimation of promoter-dependent and promoter-independent transcription rates. The dynamical range of the promoter-independent transcription rates was larger than that of the mRNA half-lives. The rapid mRNA turnover and the broad adjustability of promoter-independent transcription rates are expected to have a major impact on stochastic gene expression and gene network behavior.

INTRODUCTION

The turnover of eukaryotic mRNAs involves multiple steps. The mRNAs synthesized by the polymerase are capped at their 5′-end and polyadenylated at their 3′-end [poly(A) tail]. The degradation of canonical mRNAs occurs largely in the cytoplasm and begins with the removal of the poly(A) tail (*1*–*3*). Subsequently, mRNAs are processed either by the Xrn1p-mediated 5′ to 3′ degradation pathway after decapping or by the exosome (3′ to 5′) without decapping. Despite this complexity, mRNA degradation profiles typically match a simple exponential decay, which allows an efficient estimation of mRNA half-lives (*4*).

Even though yeast *Saccharomyces cerevisiae* is a powerful model organism to study mRNA decay, few sequences have been identified that have a consistent effect on mRNA stability, constitutively or in response to environmental factors (*5*, *6*). The answer to this apparent contradiction may lie in the fact that the different methods of half-life measurements yield different results. Not only the average half-lives differ but also the correlation between half-lives measured with these methods is generally very low (*7*, *8*). Thus, different methods classify different mRNAs as stable and unstable, which hampers the identification of stability sequence motifs.

Three main classes of methods have been available to measure RNA half-life: in vivo labeling (metabolic labeling), general inhibition of transcription by drugs or mutation, and transcriptional control by regulatable promoters (*4*). Transcriptional control and transcriptional inhibition are related methods because gene expression is shut off and the mRNA level starts to decline. The two methods differ with respect to the scale of inhibition. With transcriptional inhibition, the expression of all genes is inhibited. On the other hand, the expression of a single gene is stopped with transcriptional control.

To perform the metabolic labeling (also known as pulse chase), the cells are first exposed to a pulse of modified nucleotides, which are then incorporated into the newly synthesized RNAs. During the chase period, the modified nucleotides are washed out and replaced by natural nucleotides, following which the amount of the labeled mRNAs declines. Pulse chase and transcriptional inhibition can be used for genome-wide measurements.

Biozentrum, University of Basel, 4056 Basel, Switzerland.
*These authors contributed equally to this work.
†Corresponding author. Email: attila.becskei@unibas.ch

Each method has its own potential disadvantages (*4*). A poor signal-to-noise ratio and the load of the modified nucleotides may limit the accuracy of the measurement with metabolic labeling, whereas transcriptional inhibition may alter the stability of specific mRNAs.

Most of the studies on mRNA stability in yeast have used polymerase inhibition (*4*). However, recent experimental evidence suggests a global interdependence between the transcription and degradation machinery (*9*). For example, if the polymerase is mutated or inhibited, the mRNAs become stabilized. Positive and negative feedback has been proposed to explain this interdependence (*10*, *11*). This interdependence may explain the lack of correlation between the different methods (*8*).

Here, we devised a gene-specific method to shut off gene expression, which has been recommended to study mRNA degradation to avoid potential perturbations by global transcriptional inhibition or metabolic labeling (*4*). This method, which we named multiplexed gene control (MGC), reveals that mRNA turnover is very fast compared to the previously published estimates. To validate this finding, we performed experiments with different methodologies.

In the second part of this work, we calculated mRNA synthesis rates (transcription rates) and took advantage of the fact that promoter replacement decouples regulation by the promoter from regulation by the DNA sequence that encodes the mRNA. In this way, we were able to compare the dynamic ranges of promoter-dependent and promoter-independent transcription rates.

RESULTS

Multiplexing with tagged mRNAs enables fast and reliable half-life measurements

To shut off the expression of individual genes in *S. cerevisiae*, we placed genes under the control of a modified *GAL1* promoter, $P_{[tetO]4in\mathit{GAL1}}$, in which the four binding sites for the transcriptional activator Gal4p were replaced with *tet* operators (Fig. 1A). The downstream part of the *GAL1* promoter was truncated to permit the inclusion of the 5′ untranslated region (5′UTR) of the endogenous gene (tables S1 to S3). Gene expression is then regulated by the tetracycline transactivator (tTA), also known as the Tet-OFF system: Addition of doxycycline dissociates tTA from the operators and consequently shuts off expression (*4*).

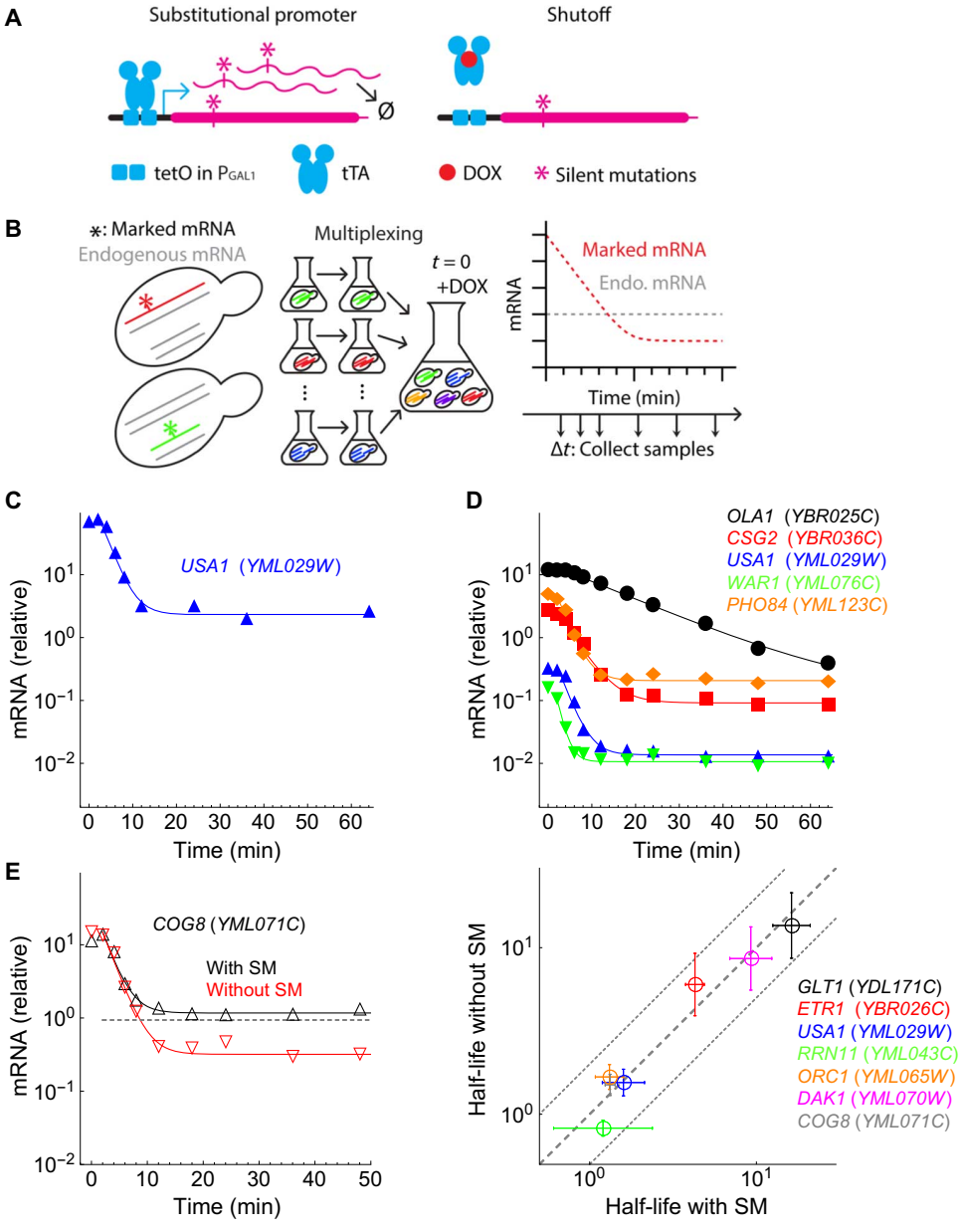

Fig. 1. Design of MGC to measure mRNA half-lives. (**A**) The endogenous promoter is substituted with $P_{[tetO]4inGAL1}$, and silent mutations mark the RNA expressed under the control of tTA. (**B**) The introduction of silent mutations permits multiplexed measurements so that the expression of the endogenous gene allele is maintained to prevent the pleiotropic effects of shutting down expression. (**C** and **D**) Time course of mRNA decay in experiments using single (C) or multiplexed (D) shutdown. The two half-lives are in good agreement (1.67 and 1.66 min). Five decay curves are shown from a single multiplexed experiment pooling 10 strains. (**E**) The silent mutations (SM) do not alter half-lives, as evidenced by comparing the decay of mRNAs with and without silent mutations in haploid cells. The dashed gray line in the left panel indicates the expression of endogenous *COG8*. The gray dashed line in the right panel indicates the expected equality of the two decay rates, and the dotted lines indicate a twofold departure from this equality. Error bars represent SD (n = 3 or 4).

Doxycycline is known to have minimal or no effect on gene expression in yeast (*12*).

To permit multiplexing of the measurement, we tagged the mRNA expressed under the control of the $P_{[tetO]4inGAL1}$ with silent (synonymous) mutations. Introducing four synonymous point mutations in the 5′ part of the coding sequence was sufficient to distinguish the tagged mRNA from the endogenous mRNA with quantitative polymerase chain reaction (qPCR) (see the "RNA extraction, reverse transcription, and qPCR" section in Materials and Methods and tables S4 to S6). One allele of a single gene was tagged in each strain. This setup has two advantages. First, the endogenous [wild-type (wt)] allele is expressed in diploid cells even after the expression of the tagged allele is shut down, which permits the study of essential genes without pleiotropic effects. Second, when multiple strains are pooled together and expression is measured by qPCR, each tagged allele can be distinguished from the wt allele at the homologous chromosomes of the same strains and the wt alleles of other pooled strains (Fig. 1B).

To acquire precultures for use in our MGC experiments, we first grew each yeast strain separately; each strain had mRNA. Subsequently, we pooled typically 5 to 10 precultures in equal proportions before shutting off gene expression by the addition of doxycycline. The decay profiles for a single strain and pooled strains are very similar (Fig. 1, C and D, and data file S1, *USA1* mRNA). The multiplexing considerably reduced the time required to measure the half-lives of multiple mRNA species because both RNA isolation and reverse transcription were performed with the pooled strains. Furthermore, the replicated experiments have a low variability, with a coefficient of variation (CV) of 16% (data files S2 and S3).

Although large-scale alterations in codon usage may alter mRNA half-life (*13*), we did not expect changes in the mRNA half-lives in MGC because we introduced only a few silent (synonymous) point mutations. Measuring the half-lives of randomly selected mRNAs with shorter and longer half-lives revealed that the synonymous mutations (Fig. 1E) did not cause more than a 1.5-fold change in the measured decay rate.

Similarly, there was little difference between the half-lives measured in haploid and diploid cells or with different reference genes (fig. S1). Neither mRNA half-life (fig. S2) nor cell growth rate (fig. S3) was affected by the integrated plasmid sequences.

The median mRNA half-life is considerably shorter than previous estimates

We chose two chromosome segments, one each on two different chromosomes. We tagged 47 genes in these two segments. Furthermore, we included five control mRNAs, which we used for specific experiments in this study. The median mRNA half-life was 2.00 min (mean, 3.40 min; total number of measured mRNAs, $n = 52$). The distribution of the mRNA half-life was right-skewed, indicating the existence of a few mRNAs with long half-lives (Fig. 2A). We also have chosen to measure the *PGK1* mRNA known for its stability (*5*). We obtained long half-life for *PGK1* mRNA (21 ± 11 min) in our assay.

Next, we examined how the half-life estimates correlated between the different methods (Fig. 2B). For this purpose, we calculated the Spearman's rank correlation coefficient (r_s) between the MGC and the genome-wide studies. We included the following variants of the transcriptional inhibition method: temperature-sensitive *rbp1-1* allele (*14*), transcriptional inhibition with phenanthroline (*15*), anchor-away of the RNA polymerase (*7*), and a study that measured the half-lives of total and poly(A)$^+$ RNA fractions with *rbp1-1* (*13*). We included fewer metabolic labeling studies because the first study to use this method in yeast has been published recently (*16*), followed by the dynamic transcriptome analysis (DTA) (*17*), comparative DTA (cDTA) (*11*), and RNA approach to equilibrium sequencing (RATE-seq) (*18*).

The median half-life we measured was 6 to 15 times shorter than the ones obtained in genome-wide studies (Fig. 2C). The half-lives measured in our study displayed no correlation with the global inhibition methods using the anchor-away polymerase and phenanthroline, and there was modest correlation with the rbp1-1 studies (Fig. 2B). A modest but significant correlation was found with the GRO (*19*), in which the RNA decay rate is calculated indirectly on the basis of the measured RNA synthesis rate and steady-state level of the RNA. There was a large variation in the correlation coefficients between MGC and the variants of the metabolic labeling studies. In these variants, cells are exposed to different concentrations of modified nucleotides for different periods of time (pulse duration). A high correlation was found with the cDTA ($r_s = 0.77$) and the DTA ($r_s = 0.80$) methods (Fig. 2, B and C), which use short pulses of labeled nucleotides, and the production and degradation rates are calculated by modeling (*11*). The rank correlation coefficient of 0.80 was the highest of all values of correlations calculated for all possible pairs of methods, not considering the related studies (for example, DTA and cDTA). The high correlation is quite surprising because the MGC and cDTA use completely different techniques.

To assess whether the high correlation between MGC and cDTA data sets can be used predictively, we chose two mRNAs with very long half-lives in the cDTA data set (*YJR139C*, 132.9 min; *YDR032C*, 127.4 min) and cloned the corresponding constructs. The measured half-lives (12.1 min for *YJR139C* and 10.5 min for *YDR032C*; data file S4) indicate that they belong to the group of very stable mRNAs also in the MGC data set.

Notwithstanding the high correlation, even the cDTA study reported a six times higher median half-life. The median half-lives in the cDTA study are similar when calculated for the 52 mRNAs studied in our work and for the entire yeast mRNA population (10.9 and 11.5 min, respectively), which confirms that our sampling is representative of the genome-wide distribution, and the median of our sample estimates the population median with a small margin of error (6%). Ten percent of the mRNAs have half-lives below 1.1 min. Ten percent of mRNAs have half-lives above 6.1 min, which represent the stable mRNAs.

The substitutional promoters do not affect the mRNA half-life

What may explain the difference in the median half-lives? Unlike the inhibitors and modified nucleotides used in the global methods for mRNA half-life measurements, promoter replacement in MGC is not expected to introduce global changes in cellular metabolism. Any impact on the half-life may stem from the introduced promoters. For example, the promoter can influence the decay rate of mRNA by loading factors to the mRNA, which affect their stability, but few such promoters are known (*20*).

To test the effect of the promoter substitution by $P_{[tetO]4in\mathit{GAL1}}$, we assessed the decay of mRNA upon shutting off gene expression with promoters that can be controlled endogenously or by inserting a short sequence into the endogenous promoter (Fig. 3A). First, we measured the decay of the *GAL2* mRNA, one of the few genes in yeast that can be shut down under the control of its endogenous promoter, controlled by galactose (*21*). Removing the galactose from the medium results in a half-life of 2.7 min for the endogenous *GAL2*, which is very similar to the half-life measured with the substitutional promoter (3.1 ± 0.4 min, mean ± SD, $n = 3$; Fig. 3B and data file S2). For comparison, the half-life of *GAL2* in the cDTA data set is 40.7 min.

Because the expression of most genes under the control of their endogenous promoters cannot be shut down with endogenous signal, we devised a strategy to rule out the promoter dependence of the mRNA stability, using insertional promoters. We designed promoters by inserting repressor binding sites into the promoter. In this way, the endogenous promoter sequence is retained, but the expression can be shut down after the association of the repressor to the promoter. The site of insertion has to be chosen in a way that allows efficient repression. The repressor efficiency can be markedly increased by positioning the binding sites upstream of and close to the TATA box (*22*). For this reason, we constructed insertional promoters to recruit tetR-repressor fusion proteins to *tet* operators inserted upstream of the TATA box (Fig. 3C and fig. S4), which also guarantees that the 5′UTR remains intact. The gene expression remained similar to the endogenous level in the absence of the repressor (Fig. 3D). We have tested two repressors, Ssn6p and Sum1p (*22*), to see which one shuts down gene expression

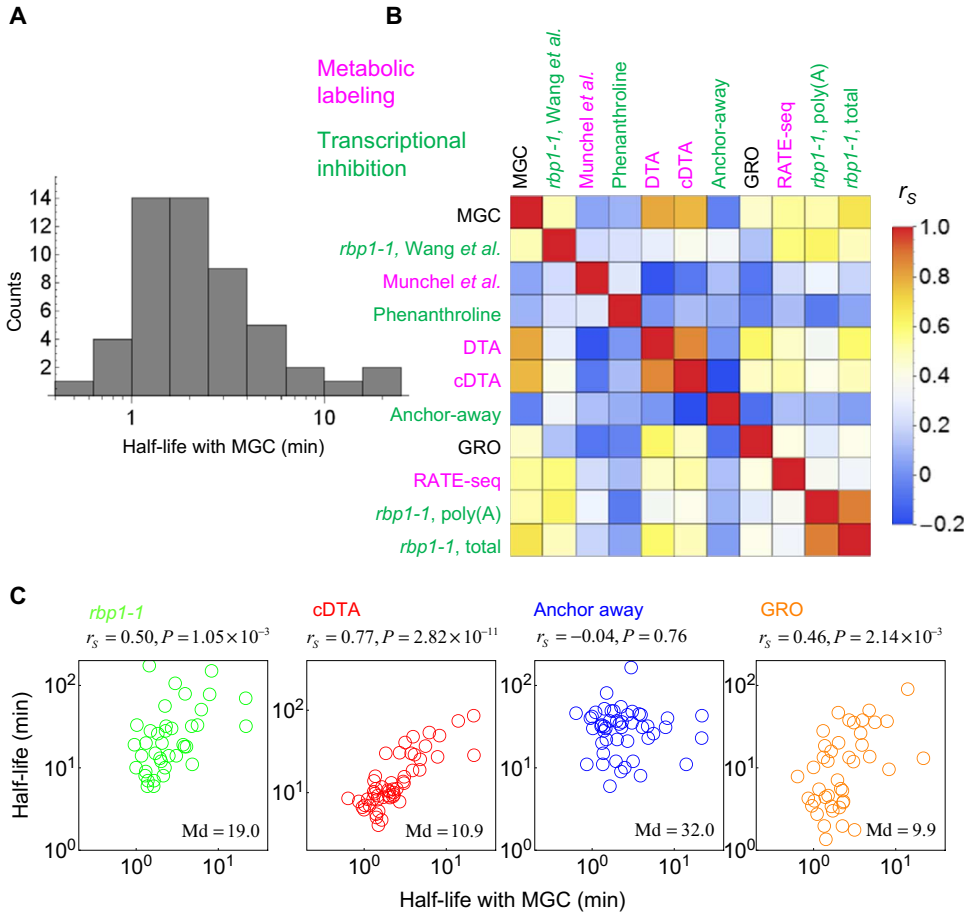

Fig. 2. MGC yields short mRNA half-lives and correlates with only one of the global methods. (**A**) Distribution of half-life using MGC. (**B**) Correlation matrix of published data sets and half-lives measured by MGC with the Spearman's rank correlation coefficient. Data from the following studies were compared (the specific method names, when available, are indicated as given in the respective study): *rbp1-1*, Wang *et al.* (*14*), Munchel *et al.* (*16*), phenanthroline (*15*), DTA (*17*), cDTA (*11*), the anchor-away (*7*), Genomic Run-On (GRO) (*19*), RATE-seq (*18*), and the study that measured the half-lives of total and poly(A)$^+$ RNA fractions with *rbp1-1* (*13*). The methods using metabolic labeling and transcriptional inhibition are shown in magenta and green, respectively. (**C**) Correlation of half-lives measured by MGC and the indicated methods (Md, median; r_S, Spearman's rho; *P*, *P* value).

more rapidly. To assess how quickly repression is established, we inserted an intron sequence into the gene to generate a precursor mRNA. The precursor mRNA level can be used to monitor rapid changes in promoter activity because splicing is fast (*23*). rtetR-Sum1p resulted in a more rapid disappearance of the precursor mRNAs, with a half-time of around 2 min (*USA1*, 1.65 ± 1.57; *GLT1*, 1.35 ± 0.84; mean ± SD, $n = 2$; see also Fig. 3E). The decay of the mRNAs expressed from the constructs with insertional and substitutional promoters was similar (Fig. 3, E and F), indicating the absence of a promoter-specific effect. The dynamic range of expression with the insertional promoter is less than that with the substitutional one, but it is still larger than one order of magnitude (Fig. 3D).

To further validate our results with an independent approach, we imaged cells with the substitutional promoters using single-molecule fluorescence in situ hybridization (smFISH) (*24*) to distinguish nascent transcripts and mature mRNAs. If a promoter that affects mRNA degradation is replaced, the mature mRNA level in the cytoplasm is expected to change relative to the nascent site, where the mRNA being synthesized is tethered to the DNA. Thus, the nascent-to-mature mRNA ratio is useful to characterize the promoter dependence of mRNA stability because it is not affected by variations in the transcription rate (see Materials and Methods). Therefore, we measured the ratio of mature to nascent mRNAs expressed under the control of the $P_{[tetO]4inGAL1}$ or the endogenous promoter. By comparing endogenous mRNAs with tagged mRNAs under the control of the substitutional promoters, we observed very similar ratios for a random selection of genes (Fig. 4).

The above three independent experiments indicate that MGC experiments reflect mRNA half-lives faithfully. What may explain then the long half-lives measured with the other methods? The discrepancies may be explained by the stress response elicited by global transcription inhibition or by modified metabolites or may be due to the introduction of a time-limiting step. For example, the number of P bodies increased after the addition of phenanthroline—a sign of the stress response (fig. S5).

Half-life estimates have a major impact on the deterministic and stochastic behavior of gene networks

We wanted to see the impact of the mRNA half-life on the behavior of gene networks. It is important to note that mRNA half-lives are significantly shorter than protein half-life, which is around 40 min in budding yeast in dividing cells (*25*), and may be even longer (8 hours) in nondividing cells (*26*). Therefore, the behavior of a typical

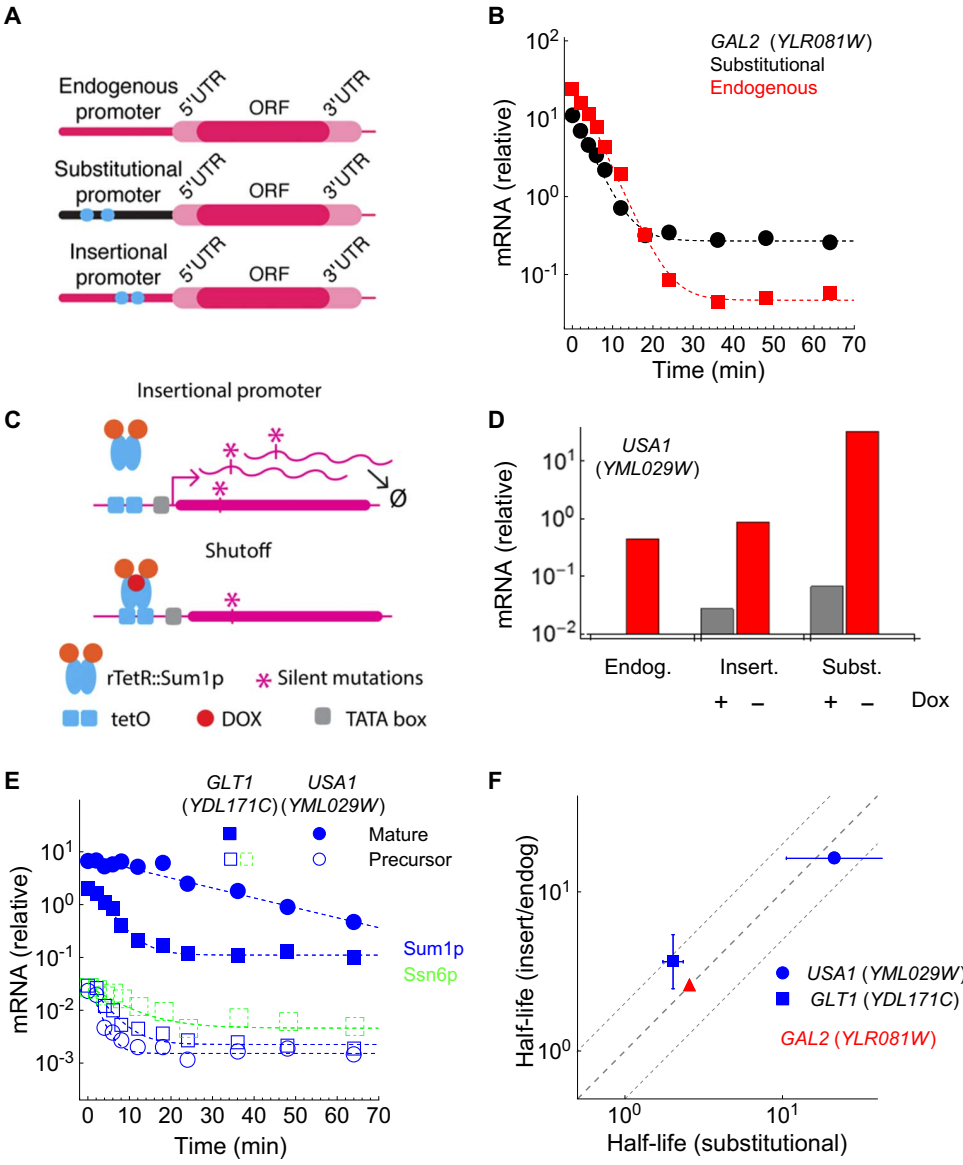

Fig. 3. Lack of promoter dependence of mRNA decay assessed by endogenous and insertional promoters. (**A**) Scheme of the endogenous, substitutional, and insertional promoters. (**B**) Time course of the decay of the YLR081W (*GAL2*) mRNA driven by its endogenous promoter (shut down by galactose removal; $t_{1/2}$ = 2.6 min) or driven by the substitutional promoter ($t_{1/2}$ = 2.6 min). (**C**) Two *tet* operators were introduced upstream of the TATA box in the endogenous promoter to create the insertional promoters. (**D**) *USA1* mRNA expression driven by the respective promoters. Dox, doxycycline. (**E**) Decay profiles of the precursor and mature mRNAs of the *GLT1* and *USA1* genes upon dissociation of TetR-Sum1 (blue). The addition of doxycycline results in a slow deinduction kinetics with TetR-Ssn6, evidenced by the long half-time (5.2 min; green) of the *GLT1* precursor mRNA. (**F**) Comparison of half-lives obtained with substitutional promoters to that with the endogenous (*GAL2*) or insertional promoters (*USA1* and *GLT1* mRNAs). The decay of the mature mRNA was not affected by splicing (*USA1* with intron, $t_{1/2}$ = 2.6 min; *USA1* without intron, $t_{1/2}$ = 2.0 min).

network is expected to be dominated by protein turnover and not by mRNA turnover. We compared deterministic models with short and long mRNA half-lives (1 and 10 min). Modeling of the induction kinetics of a single gene revealed that the mean response time of the protein was only 1.5 times slower with the more stable mRNA, which confirms the previous expectation (figs. S6A and S7). However, the same shift in half-life resulted in a four times slower response time of the protein if gene expression is controlled by negative feedback (fig. S6B). This finding was robust with respect to the value of protein half-life (40 min and 8 hours). Thus, mRNA half-lives can strongly influence the behavior of simple regulatory networks even if protein half-lives are considerably longer.

Gene expression is noisy, especially when monitored at the single-molecule mRNA level (*27*, *28*). mRNA turnover also plays an important role in models of stochastic gene expression (*29*). We analyzed the molecule copy number distributions of five mRNAs, obtained by smFISH. The CV of the distribution is a common measure of noise in gene expression. The noise was relatively uniform, with a CV ranging from 0.5 to 0.65, the only exception being the *PIF1*, which had higher noise levels: CV (endogenous), 0.8; CV (substitutional), 0.94. Thus, the substitutional

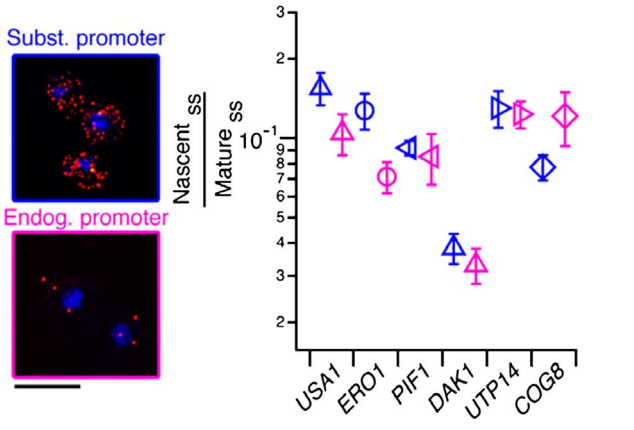

Fig. 4. The cytoplasmic decay rate of mRNA is not affected by promoter replacement, as determined by smFISH. (**Left**) Representative pictures of smFISH for mRNAs driven by the substitutional promoter (blue) or by their endogenous promoters (magenta). Scale bar, 5 μm. (**Right**) Ratio of nascent to mature mRNAs expressed under the control of endogenous and substitutional promoters. Error bars are SD of duplicate measurements.

gene mirrors the noise of the endogenous counterpart (table S7). Next, we fitted the widely used two-state promoter model of gene expression (*30*) to the observed distributions (see Materials and Methods and fig. S8). The two-state model describes the active and inactive states of the promoter, and the transition between the two states can be triggered by the binding of a transcription factor (TF) to the promoter. Thus, the switching rates between the two states (k_{ON} and k_{OFF}) reflect the kinetics of the TF binding.

We obtained good fits independently of whether the MGC or the cDTA half-lives were used in the model (Fig. 5, A and B). However, the estimated promoter activation (k_{ON}) was faster when the shorter half-lives of the MGC data set were used (Fig. 5, C and D). The ratio of the two half-lives was comparable to that of the respective fitted k_{ON} values. This proportionality is particularly evident for the tTA-driven mRNAs (Fig. 5D). Assuming that there is a single binding site in the promoter, a 10-fold increase in the k_{ON} values translates into a 10 times faster association rate of the activator to the promoter. Thus, parameter estimates for TF binding kinetics will considerably depend on the RNA half-life estimates. These two examples using deterministic and stochastic models suggest that the goodness of model predictions and parameter estimation will strongly depend on the correctness of mRNA half-lives.

Degradation of unstable mRNAs depends strongly on *XRN1*

We examined how the main decay pathway affects the variability in the mRNA decay rates. Xrn1p is the nuclease that degrades the mRNA in the 5′ to 3′ direction and is considered to represent the main pathway of mRNA degradation (*31*). To examine the decay rates in the *xrn1* deletion strains, we have selected four stable mRNAs (half-life, >5 min) and four mRNAs with typical or short half-lives (1 to 2 min). Both groups were more stable in the *xrn1*Δ background, with half-lives ranging from 8 to 30 min (Fig. 6, A and B). However, the mRNAs with short half-lives become considerably more stabilized (see *WAR1*, *COG8*, *USA1*, and *HMT1* mRNAs and their perpendicular distance to the dashed line, which represents no change; Fig. 6B). A similar trend in stabilization of mRNAs was observed when we compared the half-lives of the endogenous GAL genes in wt and *xrn1*Δ backgrounds, after washing out galactose (Fig. 6C). This suggests that *XRN1*—directly or indirectly—explains a substantial part of the variations in the mRNA stability.

Crucial role of the RNA coding sequence is evidenced by assessing the promoter dependence of the RNA synthesis rates

The benefit of our method is that it provides information not only on the decay rates but also on the promoter dependence of RNA synthesis rates. We also calculated the transcription rates of the endogenous genes. The transcription rates of the endogenous and promoter-replaced genes correlate weakly, suggesting that the promoter and the DNA sequence encoding the RNA can control the transcription rates independently (Fig. 6, D and E). The rates of mRNA synthesis under the control of identical substitutional promoters vary broadly (Fig. 6E). To quantify the dynamic ranges of these rates, we used the 90:10 quantile ratio (that is, decile ratio), which is the rate at the 90th percentile divided by the rate at the 10th percentile. The 10th and 90th percentiles of the synthesis rates are 0.0036 and 0.203 RNA molecules/min, respectively, for the endogenous genes (see the "Digital PCR" section in Materials and Methods). The 90:10 ratio was 12 and 46 for the RNA synthesis rate under the control of the substitutional and endogenous promoters, respectively. In comparison, the 90:10 ratio of the RNA half-lives is 7 (Fig. 6F). Thus, the dynamic range of the transcription rates determined by the DNA sequence that encodes the RNA is larger than that of the mRNA half-lives.

DISCUSSION

It has been repeatedly observed that the half-life estimates obtained by metabolic labeling and transcriptional inhibition methods display low or no correlation, that is, different mRNAs are classified as stable and unstable (*7*, *8*). Despite the discordant data, little effort has been made to compare these methods to the independent ones. Substantially more effort has been invested in the systematic comparison of methods in other fields, exemplified by the validation of methods to study protein-protein interactions (*32*–*34*).

It is surprising that even different variants of the same class of method can display large variations. The half-life estimates with MGC did not correlate with those of the classical pulse-chase method (*16*) but did correlate with cDTA. RNA is labeled with 4-thiouracil (4TU) in both the classical pulse chase and cDTA methods. However, cells are exposed to a higher 4TU concentration with cDTA, but for a shorter period of time (pulse labeling). Having a short pulse may eliminate or reduce the toxicity due to modified nucleotides. Analogously, different variants of transcriptional inhibition yield distinct results. Although there is no correlation between MGC and transcriptional inhibition by anchor-away, there is a modest but significant correlation between the MGC data and inhibition by the *rbp1-1* allele. The fact that the details of the experimental protocol matter are also illustrated by the observation that the degree of the inhibitor-dependent mRNA stabilization strongly depends on the concentration of the added thiolutin, a transcriptional inhibitor (*35*).

The highest correlation was found between two distinct methods: Our half-life estimates were highly correlated with those obtained with the cDTA method, which means that both methods tend to classify the same mRNAs as stable or unstable. At the same time, the MGC experiments yielded a median half-life of around 2 min, which is around five to six times shorter in comparison with the cDTA data (*11*).

We performed two experiments to show that the short half-life in MGC is not due to promoter replacement. A unique form of validation can be performed with those genes whose expression can be shut down by modulating a natural signal. This is possible with very few genes in yeast, such as the GAL genes; the half-life of *GAL2* mRNA was similar with endogenous and substitutional promoters. Similarly, the data

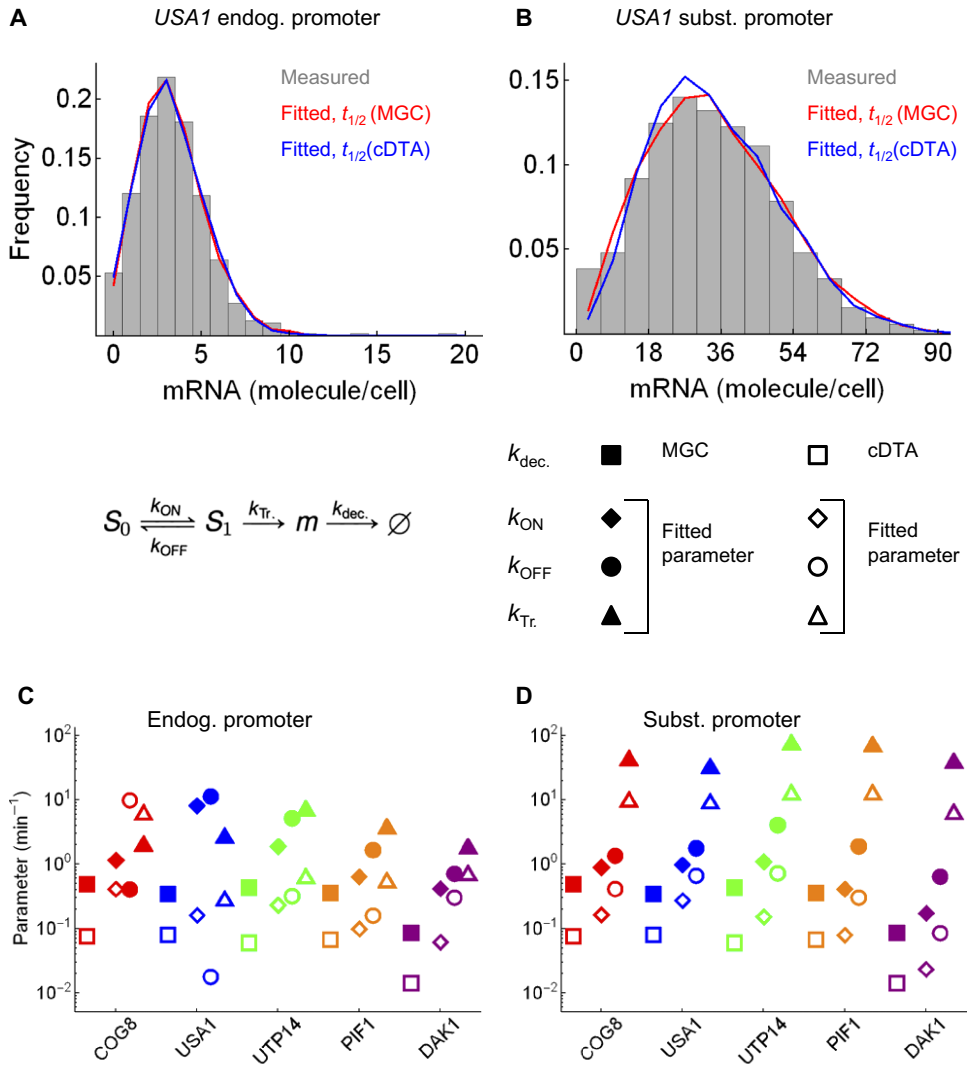

Fig. 5. Correct mRNA half-life estimation is of critical importance for stochastic models. (**A** and **B**) Histogram of *USA1* mRNA copy number distribution (smFISH) under the control of the endogenous (A) or substitutional (B) promoter and fitted distribution using either MGC (red) or cDTA (blue) half-life estimates. (**C** and **D**) Parameters estimated for the two-state promoter model (k_{ON}, k_{OFF}, and k_{Tr} rates) are shown for models assuming the two different decay rate constants for the endogenous (C) or substitutional (D) promoter.

sets obtained with insertional and substitutional promoters were consistent (Fig. 3F). The insertion of the *tet* operators did not considerably change the expression level, which indicates that the binding of the endogenous TFs to the promoter was not perturbed by the insertion (Fig. 3D).

In addition to the validation of half-lives with endogenous and inserted promoters, two considerations can explain the high correlation, despite the difference in median half-lives between MGC and cDTA: the use of a scaling factor in cDTA, and the stabilization of mRNA by transcriptional inhibition. The cDTA half-life estimates are obtained by model fitting, which incorporates a linear scaling factor, which may be influenced by the rates of cellular uptake and incorporation of labeled nucleotides into the mRNA. The rate of these processes is often unknown, and it is rather difficult to determine. Studies in yeast indicate that the intracellular accumulation of small molecules can be slower than expected (*36*). When such a slow transient process is taken into account, a linear shift in the system behavior can be observed. Therefore, it is plausible that a slow transport of the nucleotides explains a linear increase of the mRNA half-lives estimated by cDTA. Our MGC method provides, in principle, a convenient approach to estimate the scaling factors for cDTA, especially when it is tested in new organisms and conditions.

A study that examined the effect of transcriptional inhibition on the stability of the mRNAs (*11*) provides a second line of evidence for the fast mRNA turnover. It was shown that the small-molecule phenanthroline not only inhibits transcription but also reduces mRNA decay rates measured by cDTA. Furthermore, there is a nearly linear relationship between synthesis and degradation rates measured in different genetic mutants that affect mRNA turnover. These observations can then be applied to transcriptional inhibition by thermal inactivation of the *rbp1-1* allele: Transcription is inhibited by around 10-fold (*14*). The above linear relationship suggests that a 10-fold transcriptional inhibition induces a 10-fold stabilization of the mRNAs. Most transcriptional inhibition studies (using *rbp1-1* or phenanthroline) report half-lives in

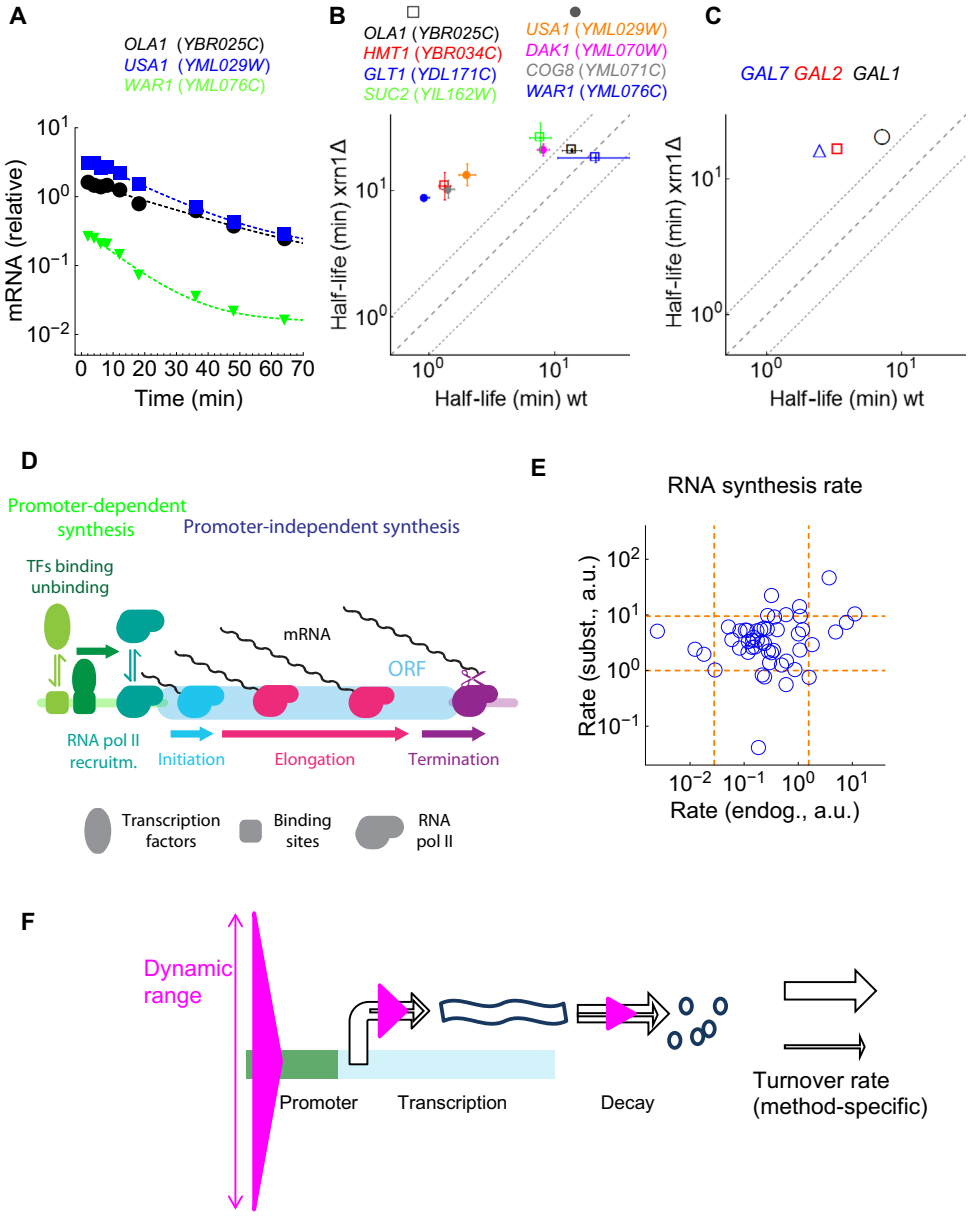

Fig. 6. Determinants of variability in the mRNA decay rate and promoter-independent variation in RNA synthesis rate. (**A** and **B**) Time courses for and half-lives in *xrn1*Δ and wt cells, determined using MGC. The dashed line represents the expected equality, and the dotted lines are twofold deviations from this equality. Error bars represent the SD of duplicate measurements, except for *DAK1*, *USA1*, and *COG8*, which were triplicated. (**C**) Comparison of half-lives of the endogenous GAL mRNAs in *xrn1*Δ and wt cells after galactose washout (right). (**D**) Scheme of processes contributing to variations of promoter-dependent (green) and promoter-independent (blue-magenta) mRNA synthesis rate. RNA pol II, RNA polymerase II. (**E**) mRNA synthesis rates under the control of the substitutional and endogenous promoters. The dashed orange lines represent the 0.1 and 0.9 quantiles of the synthesis rates (r_s = 0.16; P = 0.24). a.u., arbitrary units. (**F**) The bases of the magenta triangles are scaled to represent the dynamic range of promoter-dependent and promoter-independent mRNA synthesis rates and the mRNA decay rates, expressed as the 90:10 quantile ratio. The width of the black arrows indicates the turnover rates.

the range between 10 and 25 min. Thus, a correction for a 10-fold stabilization would yield a median estimate of around 1 to 2.5 min, which indirectly underpins our median half-life estimates. It is likely that not all mRNAs are stabilized equally, as evidenced in our results with the *xrn1* deletion mutant. Such a differential stabilization may explain the lower correlation between the *rbp1-1* study and the MGC/cDTA studies.

The distribution of half-lives is right-skewed, that is, most mRNAs have short half-lives ($t_{1/2}$ = 1 to 2 min), and only around 20% of the mRNAs display higher stability ($t_{1/2}$ > 5 min). This may indicate that a prototypical mRNA undergoes fast degradation, and specific elements are required for an mRNA to become stable, exemplified by the *PGK1* stability element. *PGK1* is the most stable mRNA in our study. The *PGK1* mRNA is also one of the more stable mRNAs in the *rbp1-1* study (Fig. 2C, rightmost point). This specific behavior of the *PGK1* mRNA may explain why it has served as the model mRNA to identify molecular mechanisms that destabilize mRNAs, exemplified by the nonsense-mediated decay (*37*).

It remains to be seen if mRNA turnover has been underestimated also in other organisms, such as bacteria or mammalian cells. Different variants of metabolic labeling studies reported different half-lives in mammalian cells (*38*, *39*). The MGC can be, in principle, used also in other organisms either with substitutional promoters controlled by activators or with insertional promoters controlled by repressors. It will be important to perform the necessary kinetic control experiments: The half-time of precursor mRNA during splicing has to be evaluated to see if the deactivation or repression is sufficiently rapid—an essential requirement for reliable kinetic measurements.

An interesting outcome of our study was the broad dynamical range of the promoter-independent control of transcription rates (Fig. 6, E and F). The promoter is characterized by a large combinatorial repertoire of TF (activator and repressor) binding sites and core promoter sequences, including the TATA box (*40*–*42*), which permits tuning of the transcription rate within a broad range. We observed that the expression of most of the endogenous genes is distributed over a 40-fold range. When the same promoter was placed upstream of each of these genes [that is, transcription unit: open reading frame (ORF) and the flanking UTRs], we still observed a 12-fold range with a low correlation ($r_s = 0.16$) with the endogenous expression levels. This low correlation implies that a gene can have low expression under the control of a substitutional promoter but high expression under the control of its endogenous promoter, and vice versa. The position effect typically explains around two- to threefold variations (*43*, *44*). Thus, the remaining variation is likely to arise from differing efficiencies of transcriptional initiation, elongation, and termination (Fig. 6D) (*45*–*48*), explaining the large dynamical range of promoter-independent transcription rates.

These processes are expected to have a major impact on stochasticity in gene expression (*49*, *50*), which may have been underappreciated because most studies focused on the promoter dependence of stochastic gene expression. Stochastic gene expression is also strongly affected by mRNA half-life. The same mRNA distribution in single cells can be explained with both slow and fast mRNA turnover. However, a fast turnover implies that the promoter is activated and inactivated more frequently.

We found that the *PIF1* mRNA has a higher noise level than the other mRNAs examined by smFISH, independently of whether it is driven by the endogenous or the substitutional promoter (table S7). This promoter independence of noise underpins the role of cotranscriptional or posttranscriptional processes in noise. The *PIF1* mRNA has alternative start codons and is translated into two different proteins: One is localized to the mitochondria, and the other, whose translation begins at the second AUG in the ORF, is destined for the nucleus (*51*). Because translation initiation can affect mRNA degradation (*13*), it is plausible that the dual translation of the mRNA accounts for the high noise in the *PIF1* mRNA. We expect that the use of correct half-life estimates and degradation model will be essential to unveil the regulation of mRNA stability and the determinants of noise.

MATERIALS AND METHODS

Plasmids, yeast growth, and shut-off experiments

The plasmids constructed in this study are listed in table S1. The plasmids were chromosomally integrated into BY4741 and BY4743 (table S2), which are derivatives of the S228C strain of the yeast *S. cerevisiae*. tTA was constitutively expressed, driven by the P_{CLN3} promoter.

Cells were grown in synthetic complete medium (2% raffinose and 0.005% glucose). This medium provided a neutral carbohydrate condition for carbohydrate-sensitive mRNAs. The overnight cultures of the strains expressing the tagged mRNAs were refreshed at OD_{600} (optical density at 600 nm) = 0.1 until they reached an $OD_{600} \sim 0.5$. For single mRNA shutoff, doxycycline was added to the medium (final concentration, 10 μg/ml) to shut off gene expression driven by tTA, whereas for the MGC cells, cultures were pooled in a single tube before the addition of doxycycline. Samples were collected in methanol and kept on dry ice. RNA was extracted as described below. For the RNA decay rates, cultures were sampled at −15, −5, 2, 4, 6, 8, 12, 18, 24, 36, 48, and 64 min. For the extended sampling, time points of −15, −5, 6, 12, 24, 36, 48, 60, 90, 150, 180, and 240 min were included.

Gene selection for promoter disruption

We randomly selected genes in the regions 11 to 217 kb of chromosome XIII, and 281 to 411 kb of chromosome II, excluding dubious ORFs, split genes, ribosomal genes, transposons, and those genes that have a length less than 600 base pairs (bp). This length (600 bp) results from the 500-bp cloned sequence in the plasmid and 100 bp required for reverse transcription. Two 5′UTR data sets (*52*, *53*) were considered to clone UTRs. The Pelechano data set reports heterogeneous 5′UTR lengths. In contrast, the Nagalakshmi data set has unique 5′UTR lengths.

Normally, we have cloned a 5′UTR with a length defined by the mean + 1 SD according to Pelechano *et al.* (*52*). There were two types of exceptions from this rule. (i) When the 5′UTR was shorter than 100 bp, we cloned a 100-bp sequence upstream of the start codon. (ii) If there was a large heterogeneity in 5′UTR lengths (SD/mean > 1), we have chosen the Nagalakshmi data set for the cloning due to the lower variability (fig. S9). Lengths of the 5′UTRs cloned are shown in table S3.

Chromosomal integration of substitutional promoters

All plasmids were constructed as described in fig. S10. Briefly, we used pRS306 (*54*) as backbone. The Gal4p binding sites in the *GAL1* promoter were replaced by *tet* (version 2) operators (magenta ovals), and the *GAL1* promoter was truncated 12 bp downstream of the TATA box. The 5′UTR and the truncated ORF of each gene (the homologous gene sequence) constituted the homologous sequence for integration. The four synonymous mutations were located 50 bp downstream of the start codon. We also added a restriction site (RS) for linearization of the plasmid by fusion PCR so that cloning can be performed with a single final PCR product. The RS was located around 200 bp downstream of the silent mutations to avoid recombinational loss of the silent mutations during the integration of the plasmid (fig. S10). A 100-bp coding sequence (red box) was also included to allow efficient homologous recombination. The size of the entire homologous sequence was kept below 500 bp.

Design of the insertional promoter insertion

To shut off gene expression with the least possible change in the endogenous promoter sequence, we inserted two *tet* operators separated by 20 bp, 50 bp upstream of the identified TATA box (fig. S4) (*55*). Chromosomal integration was performed as with the substitutional promoters. Cells express a transcriptional repressor consisting of the rTetR DNA binding domain fused to Sum1p. Addition of doxycycline leads to the binding of the transcriptional repressor to the promoter. We additionally introduced an intron 12 bp downstream of the start codon. This intron was used as an internal control to indicate how quickly repression is established ($t_{1/2} = 0.96$ min); the intron has no impact on the half-life of mature mRNA (*23*).

RNA extraction, reverse transcription, and qPCR

The cells were harvested by adding 5 ml of cultures to equal volume of methanol sitting on dry ice. Total RNA was extracted using RNeasy Mini kit (Qiagen). Complementary DNA (cDNA) was synthesized using SuperScript III (Invitrogen) with gene-specific primers. A truncated mRNA is expressed, driven by the endogenous promoter. To avoid reverse transcription of these disrupted genes, reverse transcription was primed with oligonucleotides, which anneal to the sequence around 0.1 kb downstream of the gene sequence cloned into the plasmid (fig. S11).

qPCR was done in a volume of 10 µl using Kapa Master Mix (Kapa Biosystems) and Roche LightCycler 480. RNA values were corrected for amplification efficiency (tables S4 and S5).

The relative mRNA values [mRNA (relative)] represent the mRNA levels normalized to the geometric mean of *TFC1* and *UBC6* mRNAs because the expression of these two genes displays low degree of variation across different environmental conditions (*56*).

We assessed the extent to which oligonucleotides designed to detect the tagged mRNA cross-reacted with the endogenous mRNA. We performed qPCR with a cDNA template reverse-transcribed from wt mRNAs and primed it with oligonucleotides matching the tagged mRNAs. As control, we used oligonucleotides matching the endogenous (wt) mRNAs for priming. The larger the difference between the respective cycle threshold (C_t) values, the smaller the cross-reaction (table S6). For most mRNAs, the C_t difference was larger than 5 (annealing at 60°C), and for five genes, we performed the annealing at 68°C to attain a C_t difference larger than 5 (table S6). A C_t difference of 5 indicates that a cross-reaction will affect the results when the tagged mRNA decreases to below 3% (2^{-5}) of the endogenous mRNA. Because the expression of the mRNAs with the substitutional promoter (in the absence of doxycycline) was typically 10 times higher than the endogenous expression, the decaying tagged mRNAs can be measured over a 30-fold concentration range without cross-reaction even when 10 strains are pooled. We expect that multiplexing of around 30 strains still permits a reliable assessment of the half-lives because the concentration of the tagged mRNA can be detected over a 10-fold range in the time series.

Digital PCR

cDNA was synthesized using oligo-dT and SuperScript III (Invitrogen). Droplet Digital PCR was carried out using the QX100 ddPCR system (Bio-Rad), with the following oligonucleotides to detect the *GAL1* cDNA: forward primer, 5′-GCGATCTAGCAACAAAATCCGGTTTA-3′; hydrolysis probe, (FAM)-CCATTGGCCGAAAAGTGCCCGA-(BHQ-1); reverse primer, 5′-AATATTCAGTTCTCCGGTCAGAGATT-3′. The *GAL1* mRNA copy number was normalized against cell number in the linear range of detection. The cells induced by galactose had a copy number of 12.44 ± 0.71 molecules per cell, which corresponds to the relative mRNA of 95 for the *GAL1* gene. Thus, the conversion factor from relative mRNA to molecule number was 0.13.

Estimation of decay and synthesis rates

Data series of individual measurements were fitted by nonlinear regression using the function $R(t) = R_0 e^{-\gamma t} + b$, where R_0 and b stand for the RNA level at the initial time point and due to the basal expression, respectively. The fitting was performed with Mathematica (Wolfram Research). The decline in the RNA levels after adding the doxycycline started after a short lag period. Therefore, the function was fitted to the time series starting at 2 min after the addition of doxycycline (or galactose, if relevant). To compensate residuals of data points with low absolute values, a relative weighting scheme was applied ($1/Y^2$) so that nonlinear regression minimizes the sum of squares of relative distances $\left(\sum\left(\frac{R_{data} - R_{curve}}{R_{data}}\right)^2\right)$.

Each parameter (R_0, b, γ) was independently fitted in each replicate of the time course experiment. The mean decay rate (or half-life) was calculated from the three independently fitted decay rates (or half-lives). For some mRNAs, four replicate measurements were performed.

For the calculation of the mean value of the mRNA synthesis rates, replicate measurements were performed for at least five times. Outliers were detected using the 2 MADe Method (*57*).

Detection of P bodies

Cell cultures were collected at different time intervals after the addition of phenanthroline or doxycycline, quickly spun down, resuspended in 10 µl of medium, and dropped on 2% agarose pad. Images were collected using the DeltaVision microscope [fluorescein isothiocyanate (FITC) channel; exposure time, 200 ms; objective, 100×] as stack of pictures, which were deconvolved and Z-projected, for counting of *DCP2-GFP*–positive cells.

Single-molecule mRNA FISH

Overnight cultures were refreshed (OD_{600} = 0.1) and grown for 5 hours before fixation in 3.7% formaldehyde. Cell preparation and hybridization of the probes were performed as described (*24*), with the following modifications. Coverslips were poly-lysine–coated (*58*). After permeabilization of spheroplasts, the probes were applied to the samples overnight at 40°C in a humid chamber. After the hybridization of the probes and washing of the samples, cells were mounted in ProLong Gold medium (Life Technologies) and cured overnight at room temperature before imaging.

Images were acquired as stacks of optical sections at 0.2-µm intervals using a DeltaVision deconvolution microscopy system (Applied Precision) under the following conditions: 4′,6-diamidino-2-phenylindole (DAPI); FITC; Alexa 594 channels; 100% ND; bin, 1; exposure time, 80, 2000, and 500 ms, respectively; objective, 100×. Three-dimensional stacks of images were deconvolved using the DeltaVision deconvolution microscopy system and further filtered (background subtraction, median, and convolve) using ImageJ to enhance the signal-to-noise ratio of detected spots. Autofluorescence of the cells (FITC) was used to segment the pictures with ImageJ and define the cell boundaries.

To find the correct dilution for the single-molecule FISH probes, we looked for a dilution at which no dots were detected in strains lacking the target mRNA (in deletion strains). We tested three genes driven by tTA. YML029C needed to be diluted at least 1:1000, and we diluted all probes to 1:1000, except for YML061C and YML071W, for which a 1:500 dilution was used.

For smFISH, we used FISH-quant toolbox (*59*) in Matlab. The number of mature mRNAs was scored in segmented cells after the adjustment of the detection threshold. Spots located inside the nucleus (DAPI) and displaying intensity two times higher than the average spot intensity were selected and further quantified as nascent using the point-spread function superposition approach (*59*). At least 200 cells were quantified for each experiment.

Ratio of nascent to mature mRNA

The nascent mRNA (nascent) is produced at rate p. The elongation and termination process is lumped into the parameter γ_1. The nuclear mRNA is exported to the cytoplasm at a high rate, and therefore, it is

not modeled explicitly. The mature mRNA (mature) is degraded at rate γ_2.

$$\varnothing \xrightarrow{p} \text{nascent} \xrightarrow{\gamma_1} \text{mature} \xrightarrow{\gamma_2} \varnothing$$

The ratio of their steady state equals γ_1/γ_2.

$$\frac{\text{nascent}_{ss}}{\text{mature}_{ss}} = \frac{p/\gamma_1}{p/\gamma_2} = \frac{\gamma_2}{\gamma_1} = \frac{\gamma_2}{\text{const}}$$

Because the elongation and termination process is expected to be independent of the promoter, its rate is constant: Therefore, this ratio, which can be measured with smFISH, should be identical or similar for the wt cells and the cells expressing the marked mRNA under the control of the substitutional promoter.

Estimation of parameters for the two-state promoter model of stochastic gene expression

To fit the single-molecule mRNA distribution, we simulated the two-state (telegraph) model: The promoter alternates between an inactive state (S_0) and an active state (S_1) with transition rate constants, k_{ON} and k_{OFF}. mRNA (m) is produced in the active state (S_1), with rate constant k_{Tr}, and degraded, with rate constant k_{dec}. The value of k_{dec} is taken from either the MGC or the cDTA experiments.

Distributions were generated with Gillespie's stochastic simulation algorithm, using StochKit (*60*), from 10,000 runs of 1000 min for each combination of random parameter values. Random values were generated for k_{ON}, k_{OFF}, and k_{Tr} so that the predicted Fano factor (*61*) approximates the measured one, as described in fig. S8 (see also table S7). The goodness of the fit was determined by the summed squares of the residuals (SSE), which was calculated from the measured and simulated distributions with a bin width of 1 (molecule per cell) for the endogenous promoter and bin width of 6 for the substitutional promoter. To avoid overfitting, we considered an optimal range of parameter values that yield an SSE up to a 1.3-fold multiple of the smallest found SSE. We selected a realistic combination of parameter values from the above optimal range according to the following procedure.

For the endogenous promoter, a broad range of parameter values yields similarly good fits (fig. S8). To choose realistic parameters, we took into consideration that the examined genes are housekeeping genes with constitutive expression, and we expected that their promoters are saturated by the regulating TF. Therefore, we have chosen the combination of parameter values corresponding to the largest promoter saturation, $k_{ON}/(k_{ON} + k_{OFF})$.

For the substitutional promoter, the optimal range of parameter values was scattered over a smaller domain (fig. S8). We expected that the saturation of the $P_{[tetO]4inGAL1}$ by tTA is similar for each gene. Therefore, we calculated the mean value of saturation from the optimal range of parameter values for each gene. Subsequently, the average of the mean saturations of all fives genes was calculated, which we termed the global mean saturation. Ultimately, we selected the parameter combination for each gene that yields the saturation closest to the global mean saturation.

SUPPLEMENTARY MATERIALS

Supplementary material for this article is available at http://advances.sciencemag.org/cgi/content/full/3/7/e1700006/DC1

fig. S1. The cell ploidy and the choice of reference mRNAs have no impact on measured half-lives.
fig. S2. Pop-out of the chromosomally integrated plasmid is dispensable for half-life estimation of mature mRNA.
fig. S3. The doubling time of the MGC strains (red dots) is similar to that of the parent diploid strain (black line).
fig. S4. Insertional promoter strategy.
fig. S5. Phenanthroline increases the number of P bodies.
fig. S6. mRNA half-life has a major impact on response time of a protein in a negative feedback loop.
fig. S7. Degradation rates and not synthesis rates affect the response time.
fig. S8. Parameter estimation of the two state model to fit the *USA1* RNA copy number distributions.
fig. S9. Impact of 5′UTR length on the decay profiles of mRNAs with varying 5′UTR lengths.
fig. S10. Design of plasmids with substitutional promoters and the strategy for chromosomal integration.
fig. S11. Reverse transcription strategy.
table S1. Plasmid list.
table S2. Strain list.
table S3. Cloned 5′UTR lengths of genes.
table S4. qPCR primers detecting marked mRNAs and their amplification efficiencies.
table S5. qPCR primers detecting endogenous mRNAs with their efficiencies.
table S6. Cross-reaction of primers to detect the marked mRNA with the endogenous mRNAs.
table S7. Mean, Fano factor, and CV of the RNA molecule copy number distributions.
data file S1. C_t values for one of the replicate experiments of pooled strains in the MGC experiment.
data file S2. Time courses in the replicate measurements.
data file S3. mRNA (relative) levels and decay rates.
data file S4. Time courses for *YJR139C* and *YDR032C* mRNAs.

REFERENCES AND NOTES

1. N. L. Garneau, J. Wilusz, C. J. Wilusz, The highways and byways of mRNA decay. *Nat. Rev. Mol. Cell Biol.* **8**, 113–126 (2007).
2. R. Parker, RNA degradation in *Saccharomyces cerevisae*. *Genetics* **191**, 671–702 (2012).
3. V. Balagopal, L. Fluch, T. Nissan, Ways and means of eukaryotic mRNA decay. *Biochim. Biophys. Acta* **1819**, 593–603 (2012).
4. D. O. Passos, R. Parker, Analysis of cytoplasmic mRNA decay in *Saccharomyces cerevisiae*. *Methods Enzymol.* **448**, 409–427 (2008).
5. T. LaGrandeur, R. Parker, The *cis* acting sequences responsible for the differential decay of the unstable MFA2 and stable PGK1 transcripts in yeast include the context of the translational start codon. *RNA* **5**, 420–433 (1999).
6. M. Vemula, P. Kandasamy, C.-S. Oh, R. Chellappa, C. I. Gonzalez, C. E. Martin, Maintenance and regulation of mRNA stability of the *Saccharomyces cerevisiae OLE1* gene requires multiple elements within the transcript that act through translation-independent mechanisms. *J. Biol. Chem.* **278**, 45269–45279 (2003).
7. J. V. Geisberg, Z. Moqtaderi, X. Fan, F. Ozsolak, K. Struhl, Global analysis of mRNA isoform half-lives reveals stabilizing and destabilizing elements in yeast. *Cell* **156**, 812–824 (2014).
8. M. Sun, B. Schwalb, D. Schulz, N. Pirkl, S. Etzold, L. Larivière, K. C. Maier, M. Seizl, A. Tresch, P. Cramer, Comparative dynamic transcriptome analysis (cDTA) reveals mutual feedback between mRNA synthesis and degradation. *Genome Res.* **22**, 1350–1359 (2012).
9. M. Dori-Bachash, E. Shema, I. Tirosh, Coupled evolution of transcription and mRNA degradation. *PLOS Biol.* **9**, e1001106 (2011).
10. G. Haimovich, D. A. Medina, S. Z. Causse, M. Garber, G. Millán-Zambrano, O. Barkai, S. Chávez, J. E. Pérez-Ortín, X. Darzacq, M. Choder, Gene expression is circular: Factors for mRNA degradation also foster mRNA synthesis. *Cell* **153**, 1000–1011 (2013).
11. M. Sun, B. Schwalb, N. Pirkl, K. C. Maier, A. Schenk, H. Failmezger, A. Tresch, P. Cramer, Global analysis of eukaryotic mRNA degradation reveals Xrn1-dependent buffering of transcript levels. *Mol. Cell* **52**, 52–62 (2013).
12. J. A. Wishart, A. Hayes, L. Wardleworth, N. Zhang, S. G. Oliver, Doxycycline, the drug used to control the *tet*-regulatable promoter system, has no effect on global gene expression in *Saccharomyces cerevisiae*. *Yeast* **22**, 565–569 (2005).
13. V. Presnyak, N. Alhusaini, Y.-H. Chen, S. Martin, N. Morris, N. Kline, S. Olson, D. Weinberg, K. E. Baker, B. R. Graveley, J. Coller, Codon optimality is a major determinant of mRNA stability. *Cell* **160**, 1111–1124 (2015).
14. Y. Wang, C. L. Liu, J. D. Storey, R. J. Tibshirani, D. Herschlag, P. O. Brown, Precision and functional specificity in mRNA decay. *Proc. Natl. Acad. Sci. U.S.A.* **99**, 5860–5865 (2002).
15. J. Grigull, S. Mnaimneh, J. Pootoolal, M. D. Robinson, T. R. Hughes, Genome-wide analysis of mRNA stability using transcription inhibitors and microarrays reveals

posttranscriptional control of ribosome biogenesis factors. *Mol. Cell. Biol.* **24**, 5534–5547 (2004).
16. S. E. Munchel, R. K. Shultzaberger, N. Takizawa, K. Weis, Dynamic profiling of mRNA turnover reveals gene-specific and system-wide regulation of mRNA decay. *Mol. Biol. Cell* **22**, 2787–2795 (2011).
17. C. Miller, B. Schwalb, K. Maier, D. Schulz, S. Dümcke, B. Zacher, A. Mayer, J. Sydow, L. Marcinowski, L. Dölken, D. E. Martin, A. Tresch, P. Cramer, Dynamic transcriptome analysis measures rates of mRNA synthesis and decay in yeast. *Mol. Syst. Biol.* **7**, 458 (2011).
18. B. Neymotin, R. Athanasiadou, D. Gresham, Determination of in vivo RNA kinetics using RATE-seq. *RNA* **20**, 1645–1652 (2014).
19. V. Pelechano, S. Chávez, J. E. Pérez-Ortin, A complete set of nascent transcription rates for yeast genes. *PLOS ONE* **5**, e15442 (2010).
20. T. Trcek, D. R. Larson, A. Moldón, C. C. Query, R. H. Singer, Single-molecule mRNA decay measurements reveal promoter- regulated mRNA stability in yeast. *Cell* **147**, 1484–1497 (2011).
21. C. Hsu, S. Scherrer, A. Buetti-Dinh, P. Ratna, J. Pizzolato, V. Jaquet, A. Becskei, Stochastic signalling rewires the interaction map of a multiple feedback network during yeast evolution. *Nat. Commun.* **3**, 682 (2012).
22. J. Z. Kelemen, P. Ratna, S. Scherrer, A. Becskei, Spatial epigenetic control of mono- and bistable gene expression. *PLOS Biol.* **8**, e1000332 (2010).
23. M. M. Bonde, S. Voegeli, A. Baudrimont, B. Séraphin, A. Becskei, Quantification of pre-mRNA escape rate and synergy in splicing. *Nucleic Acids Res.* **42**, 12847–12860 (2014).
24. A. Raj, P. van den Bogaard, S. A. Rifkin, A. van Oudenaarden, S. Tyagi, Imaging individual mRNA molecules using multiple singly labeled probes. *Nat. Methods* **5**, 877–879 (2008).
25. A. Belle, A. Tanay, L. Bitincka, R. Shamir, E. K. O'Shea, Quantification of protein half-lives in the budding yeast proteome. *Proc. Natl. Acad. Sci. U.S.A.* **103**, 13004–13009 (2006).
26. R. Christiano, N. Nagaraj, F. Fröhlich, T. C. Walther, Global proteome turnover analyses of the Yeasts *S. cerevisiae* and *S. pombe*. *Cell Rep.* **9**, 1959–1965 (2014).
27. Y. Lin, C. H. Sohn, C. K. Dalal, L. Cai, M. B. Elowitz, Combinatorial gene regulation by modulation of relative pulse timing. *Nature* **527**, 54–58 (2015).
28. G. Neuert, B. Munsky, R. Z. Tan, L. Teytelman, M. Khammash, A. van Oudenaarden, Systematic identification of signal-activated stochastic gene regulation. *Science* **339**, 584–587 (2013).
29. J. M. Pedraza, J. Paulsson, Effects of molecular memory and bursting on fluctuations in gene expression. *Science* **319**, 339–343 (2008).
30. A. R. Stinchcombe, C. S. Peskin, D. Tranchina, Population density approach for discrete mRNA distributions in generalized switching models for stochastic gene expression. *Phys. Rev. E Stat. Nonlin. Soft Matter Phys.* **85**, 061919 (2012).
31. A. Siwaszek, M. Ukleja, A. Dziembowski, Proteins involved in the degradation of cytoplasmic mRNA in the major eukaryotic model systems. *RNA Biol.* **11**, 1122–1136 (2014).
32. C. von Mering, R. Krause, B. Snel, M. Cornell, S. G. Oliver, S. Fields, P. Bork, Comparative assessment of large-scale data sets of protein–protein interactions. *Nature* **417**, 399–403 (2002).
33. Y.-C. Chen, S. V. Rajagopala, T. Stellberger, P. Uetz, Exhaustive benchmarking of the yeast two-hybrid system. *Nat. Methods* **7**, 667–668 (2010).
34. J. Snider, M. Kotlyar, P. Saraon, Z. Yao, I. Jurisica, I. Stagljar, Fundamentals of protein interaction network mapping. *Mol. Syst. Biol.* **11**, 848 (2015).
35. V. Pelechano, J. E. Pérez-Ortín, The transcriptional inhibitor thiolutin blocks mRNA degradation in yeast. *Yeast* **25**, 85–92 (2008).
36. C. Hsu, V. Jaquet, F. Maleki, A. Becskei, Contribution of bistability and noise to cell fate transitions determined by feedback opening. *J. Mol. Biol.* **428**, 4115–4128 (2016).
37. S. W. Peltz, A. H. Brown, A. Jacobson, mRNA destabilization triggered by premature translational termination depends on at least three *cis*-acting sequence elements and one *trans*-acting factor. *Genes Dev.* **7**, 1737–1754 (1993).
38. M. Rabani, J. Z. Levin, L. Fan, X. Adiconis, R. Raychowdhury, M. Garber, A. Gnirke, C. Nusbaum, N. Hacohen, N. Friedman, I. Amit, A. Regev, Metabolic labeling of RNA uncovers principles of RNA production and degradation dynamics in mammalian cells. *Nat. Biotechnol.* **29**, 436–442 (2011).
39. B. Schwänhausser, D. Busse, N. Li, G. Dittmar, J. Schuchhardt, J. Wolf, W. Chen, M. Selbach, Global quantification of mammalian gene expression control. *Nature* **473**, 337–342 (2011).
40. T. I. Lee, N. J. Rinaldi, F. Robert, D. T. Odom, Z. Bar-Joseph, G. K. Gerber, N. M. Hannett, C. T. Harbison, C. M. Thompson, I. Simon, J. Zeitlinger, E. G. Jennings, H. L. Murray, D. B. Gordon, B. Ren, J. J. Wyrick, J.-B. Tagne, T. L. Volkert, E. Fraenkel, D. K. Gifford, R. A. Young, Transcriptional regulatory networks in *Saccharomyces cerevisiae*. *Science* **298**, 799–804 (2002).
41. S. Lubliner, I. Regev, M. Lotan-Pompan, S. Edelheit, A. Weinberger, E. Segal, Core promoter sequence in yeast is a major determinant of expression level. *Genome Res.* **25**, 1008–1017 (2015).
42. I. Mogno, F. Vallania, R. D. Mitra, B. A. Cohen, TATA is a modular component of synthetic promoters. *Genome Res.* **20**, 1391–1397 (2010).
43. P. Ratna, S. Scherrer, C. Fleischli, A. Becskei, Synergy of repression and silencing gradients along the chromosome. *J. Mol. Biol.* **387**, 826–839 (2009).
44. C. Batenchuk, S. St-Pierre, L. Tepliakova, S. Adiga, A. Szuto, N. Kabbani, J. C. Bell, K. Baetz, M. Kærn, Chromosomal position effects are linked to sir2-mediated variation in transcriptional burst size. *Biophys. J.* **100**, L56–L58 (2011).
45. T. S. Kim, C. L. Liu, M. Yassour, J. Holik, N. Friedman, S. Buratowski, O. J. Rando, RNA polymerase mapping during stress responses reveals widespread nonproductive transcription in yeast. *Genome Biol.* **11**, R75 (2010).
46. M. Yamanishi, Y. Ito, R. Kintaka, C. Imamura, S. Katahira, A. Ikeuchi, H. Moriya, T. Matsuyama, A genome-wide activity assessment of terminator regions in *Saccharomyces cerevisiae* provides a "terminatome" toolbox. *ACS Synth. Biol.* **2**, 337–347 (2013).
47. A. Samarakkody, A. Abbas, A. Scheidegger, J. Warns, O. Nnoli, B. Jokinen, K. Zarns, B. Kubat, A. Dhasarathy, S. Nechaev, RNA polymerase II pausing can be retained or acquired during activation of genes involved in the epithelial to mesenchymal transition. *Nucleic Acids Res.* **43**, 3938–3949 (2015).
48. I. Jonkers, H. Kwak, J. T. Lis, Genome-wide dynamics of Pol II elongation and its interplay with promoter proximal pausing, chromatin, and exons. *eLife* **3**, e02407 (2014).
49. M. Voliotis, N. Cohen, C. Molina-París, T. B. Liverpool, Fluctuations, pauses, and backtracking in DNA transcription. *Biophys. J.* **94**, 334–348 (2008).
50. M. Dobrzynski, F. J. Bruggeman, Elongation dynamics shape bursty transcription and translation. *Proc. Natl. Acad. Sci. U.S.A.* **106**, 2583–2588 (2009).
51. J.-Q. Zhou, E. K. Monson, S.-C. Teng, V. P. Schulz, V. A. Zakian, Pif1p helicase, a catalytic inhibitor of telomerase in yeast. *Science* **289**, 771–774 (2000).
52. V. Pelechano, W. Wei, L. M. Steinmetz, Extensive transcriptional heterogeneity revealed by isoform profiling. *Nature* **497**, 127–131 (2013).
53. U. Nagalakshmi, Z. Wang, K. Waern, C. Shou, D. Raha, M. Gerstein, M. Snyder, The transcriptional landscape of the yeast genome defined by RNA sequencing. *Science* **320**, 1344–1349 (2008).
54. R. S. Sikorski, P. Hieter, A system of shuttle vectors and yeast host strains designed for efficient manipulation of DNA in Saccharomyces cerevisiae. *Genetics* **122**, 19–27 (1989).
55. H. S. Rhee, B. F. Pugh, Genome-wide structure and organization of eukaryotic pre-initiation complexes. *Nature* **483**, 295–301 (2012).
56. M.-A. Teste, M. Duquenne, J. M. François, J.-L. Parrou, Validation of reference genes for quantitative expression analysis by real-time RT-PCR in *Saccharomyces cerevisiae*. *BMC Mol. Biol.* **10**, 99 (2009).
57. C. Reimann, P. Filzmoser, R. G. Garrett, Background and threshold: Critical comparison of methods of determination. *Sci. Total Environ.* **346**, 1–16 (2005).
58. T. Trcek, J. A. Chao, D. R. Larson, H. Y. Park, D. Zenklusen, S. M. Shenoy, R. H. Singer, Single-mRNA counting using fluorescent in situ hybridization in budding yeast. *Nat. Protoc.* **7**, 408–419 (2012).
59. F. Mueller, A. Senecal, K. Tantale, H. Marie-Nelly, N. Ly, O. Collin, E. Basyuk, E. Bertrand, X. Darzacq, C. Zimmer, FISH-quant: Automatic counting of transcripts in 3D FISH images. *Nat. Methods* **10**, 277–278 (2013).
60. K. R. Sanft, S. Wu, M. Roh, J. Fu, R. K. Lim, L. R. Petzold, StochKit2: Software for discrete stochastic simulation of biochemical systems with events. *Bioinformatics* **27**, 2457–2458 (2011).
61. J. Peccoud, B. Ycart, Markovian modeling of gene-product synthesis. *Theor. Popul. Biol.* **48**, 222–234 (1995).

Acknowledgments: We thank M. Scheidman, S. Wenk, and P. P. Escrivà for technical help. We thank A. Spang for sharing the DCP2-GFP strain. **Funding:** This work was supported by grants from the Swiss National Science Foundation (31003A_152742) and the StoNets RTD from Systems X. **Author contributions:** A. Becskei and A. Baudrimont designed the experiments and wrote the manuscript. A. Becskei, A. Baudrimont, V.J., and S.V. analyzed the data and performed the model fitting. E.C.V., S.V., A. Baudrimont, M.L., F.S., and T.W. performed the experiments. **Competing interests:** The authors declare that they have no competing interests. **Data and materials availability:** All data needed to evaluate the conclusions in the paper are present in the paper and/or the Supplementary Materials. Additional data related to this paper may be requested from the authors.

Submitted 2 January 2017
Accepted 13 June 2017
Published 12 July 2017
10.1126/sciadv.1700006

Citation: A. Baudrimont, S. Voegeli, E. C. Viloria, F. Stritt, M. Lenon, T. Wada, V. Jaquet, A. Becskei, Multiplexed gene control reveals rapid mRNA turnover. *Sci. Adv.* **3**, e1700006 (2017).

Multiplexed gene control reveals rapid mRNA turnover

Antoine Baudrimont, Sylvia Voegeli, Eduardo Calero Viloria, Fabian Stritt, Marine Lenon, Takeo Wada, Vincent Jaquet and Attila Becskei

Sci Adv **3** (7), e1700006.
DOI: 10.1126/sciadv.1700006